Formation Flying for Electric Sails in Displaced Orbits. Part I: Geometrical Analysis

Wei Wang[(1)], Giovanni Mengali[(2)*], Alessandro A. Quarta[(2)], Jianping Yuan[(1)]

[(1)] *National Key Laboratory of Aerospace of Flight Dynamics, Northwestern Polytechnical University, 710072 Xi'an, People's Republic of China*

[(2)] *Dipartimento di Ingegneria Civile e Industriale, University of Pisa, I-56122 Pisa, Italy*

Abstract

We present a geometrical methodology for analyzing the formation flying of electric solar wind sail based spacecraft that operate in heliocentric, elliptic, displaced orbits. The spacecraft orbit is maintained by adjusting its propulsive acceleration modulus, whose value is estimated using a thrust model that takes into account a variation of the propulsive performance with the sail attitude. The properties of the relative motion of the spacecraft are studied in detail and a geometrical solution is obtained in terms of relative displaced orbital elements, assumed to be small quantities. In particular, for the small eccentricity case (i.e. for a near-circular displaced orbit), the bounds characterized by the extreme values of relative distances are analytically calculated, thus providing an useful mathematical tool for preliminary design of the spacecraft formation structure.

Keywords: Electric solar wind sail, Heliocentric displaced orbits, Formation flying

Nomenclature

a	=	semimajor axis, [au]
$a_\oplus$	=	spacecraft characteristic acceleration, [$\mathrm{mm/s^2}$]
$\boldsymbol{a}$	=	propulsive acceleration, [$\mathrm{mm/s^2}$]
e	=	eccentricity
f	=	true anomaly, [rad]
$\boldsymbol{h}$	=	specific angular momentum vector, [$\mathrm{au^2/day}$]
H	=	displacement, [au]
i	=	inclination, [rad]
M	=	mean anomaly, [rad]
m	=	spacecraft total mass, [kg]
m_{pay}	=	payload mass, [kg]
N	=	number of tethers
n	=	mean motion, [rad/day]
O	=	Sun's center-of-mass
o	=	focus of displaced orbit
R	=	focus-spacecraft distance [au]
$\boldsymbol{r}$	=	spacecraft position vector (with $r = \|\boldsymbol{r}\|$), [au]
S	=	spacecraft center-of-mass

*Corresponding author

Email addresses: 418362467@qq.com (Wei Wang[(1)]), g.mengali@ing.unipi.it (Giovanni Mengali[(2)]), a.quarta@ing.unipi.it (Alessandro A. Quarta[(2)]), jyuan@nwpu.edu.cn (Jianping Yuan[(1)])

Published in Advances in Space Research, May 2017. doi: http://doi.org/10.1016/j.asr.2017.05.015

t	=	time, [days]
$\mathcal{T}_I$	=	inertial reference frame
$\mathcal{T}_P$	=	perifocal reference frame
$\mathcal{T}_R$	=	rotating reference frame
$\mathbb{T}_{RI}$	=	transformation matrix between $\mathcal{T}_R$ and $\mathcal{T}_I$
$\mathbb{T}_{R_D R_C}$	=	transformation matrix between $\mathcal{T}_{R_D}$ and $\mathcal{T}_{R_C}$
T_{ij}	=	(i,j) entry of matrix $\mathbb{T}_{R_D R_C}$
$\hat{\boldsymbol{x}}$, $\hat{\boldsymbol{y}}$, $\hat{\boldsymbol{z}}$	=	unit vectors of coordinate axes
α	=	cone angle, [rad]
α_n	=	pitch angle, [rad]
γ	=	elevation angle, [rad]
θ	=	argument of latitude of displaced orbit, [rad]
$\mu_\odot$	=	Sun's gravitational parameter, [$\mathrm{au}^3/\mathrm{day}^2$]
ρ_x, ρ_y, ρ_z	=	components of relative position vector in the chief's rotating frame, [au]
$\boldsymbol{\rho}$	=	relative position vector, [au]
Ω	=	right ascension of the ascending node of displaced orbit, [rad]
$\boldsymbol{\omega}$	=	angular velocity vector, (with $\omega = \|\boldsymbol{\omega}\|$), [rad/s]
ϖ	=	argument of periapsis of displaced orbit, [rad]

Subscripts

C	=	chief
D	=	deputy
I	=	inertial
max	=	maximum
min	=	minimum
P	=	celestial body

Superscripts

T	=	transpose
$\star$	=	extreme value
$\cdot$	=	time derivative
$\wedge$	=	unit vector

1. Introduction

The Electric Solar Wind Sail (E-sail) is an innovative propulsion concept that uses the natural solar wind dynamic pressure to generate a continuous thrust, without the need of any reaction mass nor any propellant. A spacecraft with an E-sail based propulsion system consists of a number of thin, long and conducting tethers, which are maintained at a high positive potential by means of an electron gun [1]. Over the last years, much effort has been devoted to study the physical mechanisms of the E-sail concept by means of experimental tests and through plasma dynamic simulations [2, 3]. Theoretical analysis results indicate that the E-sail thrust decays as the inverse Sun-spacecraft distance r (i.e. as $1/r$), with a decreasing rate slower than that of a classical photonic solar sail (i.e. as $1/r^2$). Due to this peculiarity, a number of mission scenarios have been analyzed using an E-sail as the primary propulsion system [4, 5, 6], especially for what concerns the preliminary analysis of interplanetary transfers where the problem is formulated within a time-optimal framework [7, 8].

Another promising application involving an E-sail based spacecraft is to observe the polar region of a celestial body by inserting the vehicle into a (closed) non-Keplerian displaced orbit [9, 10, 11], whose plane does not pass through the Sun's center-of-mass. Maintaining such a desired displaced orbit requires a continuous propulsive acceleration by suitably orienting the thrust vector direction in such a way to balance the centrifugal and gravitational components of the acceleration [12, 13, 14], for a time-span on the order of

some terrestrial years. However, the propulsive requirements for this kind of mission scenario, given in terms of maximum value of propulsive acceleration modulus necessary to maintain the displaced orbit, could be beyond the technological capabilities of an E-sail propulsion system [15].

A feasible solution to the problem is to (ideally) disaggregate the payload [16] among multiple spacecraft, with each functional module conveying the indispensable mass only. That way, with a reduction of the payload mass, the reference propulsive acceleration of an E-sail (the so called characteristic acceleration) may become significantly high [15]. In that case, a number of different spacecraft are required to operate in close proximity, that is, in a formation flight [17]. In addition, the concept of formation flying provides a means for increasing the observation capability, by arranging multiple E-sail based spacecraft so as to constitute a sort of large object with a predesigned geometry. In some cases the formation geometry is loosely defined, since the spacecraft are only required to operate within a bounded region. This arrangement is usually termed cluster flight or loosed formation [16]. Finally, a formation flying system comprised of multiple E-sails may contribute to a resolution improvement, enabling promising scientific missions such as the Mercury's magnetotail measurement [18] or the astronomical observation [19].

Existing results on spacecraft formation flying around displaced orbits are confined to cases in which the primary propulsion system is a photonic solar sail. In this context, [20, 21] have discussed the problem of a chief spacecraft that covers a heliocentric circular displaced orbit, while the deputy adjusts its thrust vector in order to track a given trajectory by means of an active control strategy.
An interesting contribution to the subject of spacecraft formation flight is given by the study of the relative motion of two spacecraft in displaced orbits using a geometrical approach [22, 23, 24]. For example, [22] analyzes the relative motion between two solar sails that cover a circular displaced orbit, using a set of (modified) displaced orbital elements. More recently, the geometrical analysis has been also applied to elliptic orbits using classical [23] or non-singular orbital elements [24]. In both cases the closed-form solution of the relative motion is parameterized in the configuration space. Note, however, that in [22, 23, 24] the problem of formation flight has never been addressed.

The aim of this paper is to study, for the first time, the formation flight of E-sail based spacecraft in displaced elliptic orbits. The analysis uses the recent E-sail thrust model [25, 26], in which the propulsive acceleration modulus and the cone angle are both parameterized with numerical fitting polynomial equations as functions of the pitch angle. The relative motion of the spacecraft is addressed in the configuration space using suitable coordinate transformations that incorporate a set of displaced orbital elements. Unlike the previous works [22, 23, 24], the formation geometry is studied assuming a small distance between the spacecraft in the formation, which allows the problem to be linearized. Accordingly, the extreme values of the relative distances can be accurately calculated in an analytical form. Maintaining a formation flight with prescribed maximum relative distance between the spacecraft requires, however, a cooperative control strategy. This problem is discussed in detail in a companion paper [27].

The paper is organized as follows. The next section briefly summarizes the mathematical model used to describe the propulsive thrust of an E-sail based spacecraft and the relations necessary for maintaining an elliptic displaced orbit. Section 3 discusses the performance requirements, in terms of characteristic acceleration as a function of the payload mass and the number of tethers. Section 4 illustrates the equation of relative motion and introduces the approximations necessary to find an analytical form of the bounds of the relative motion. A case study, discussed in section 5, shows the effectiveness of the proposed method, while section 6 contains the concluding remarks.

2. E-sail requirements for displaced orbits

The formation flying problem consists of a chief spacecraft that is required to track a heliocentric displaced orbit and a deputy spacecraft that orbits around the chief at a small distance from it. To better describe the mathematical model used in this paper, it is useful to start with some concepts recently introduced in the literature.

2.1. E-sail thrust model

Each spacecraft is assumed to be equipped with an E-sail, whose thrust model is taken from [25] and thoroughly discussed in [26]. In particular, [25] represent the more recent evolution of the E-sail model used for mission analysis purposes, whose first appearance is in the works of [1].

To summarize this thrust model, we introduce the unit vector $\hat{\boldsymbol{n}}$ normal to the nominal plane containing the sail tethers and pointing in the direction opposite to the Sun, see Fig. 1. According to [25], the E-sail

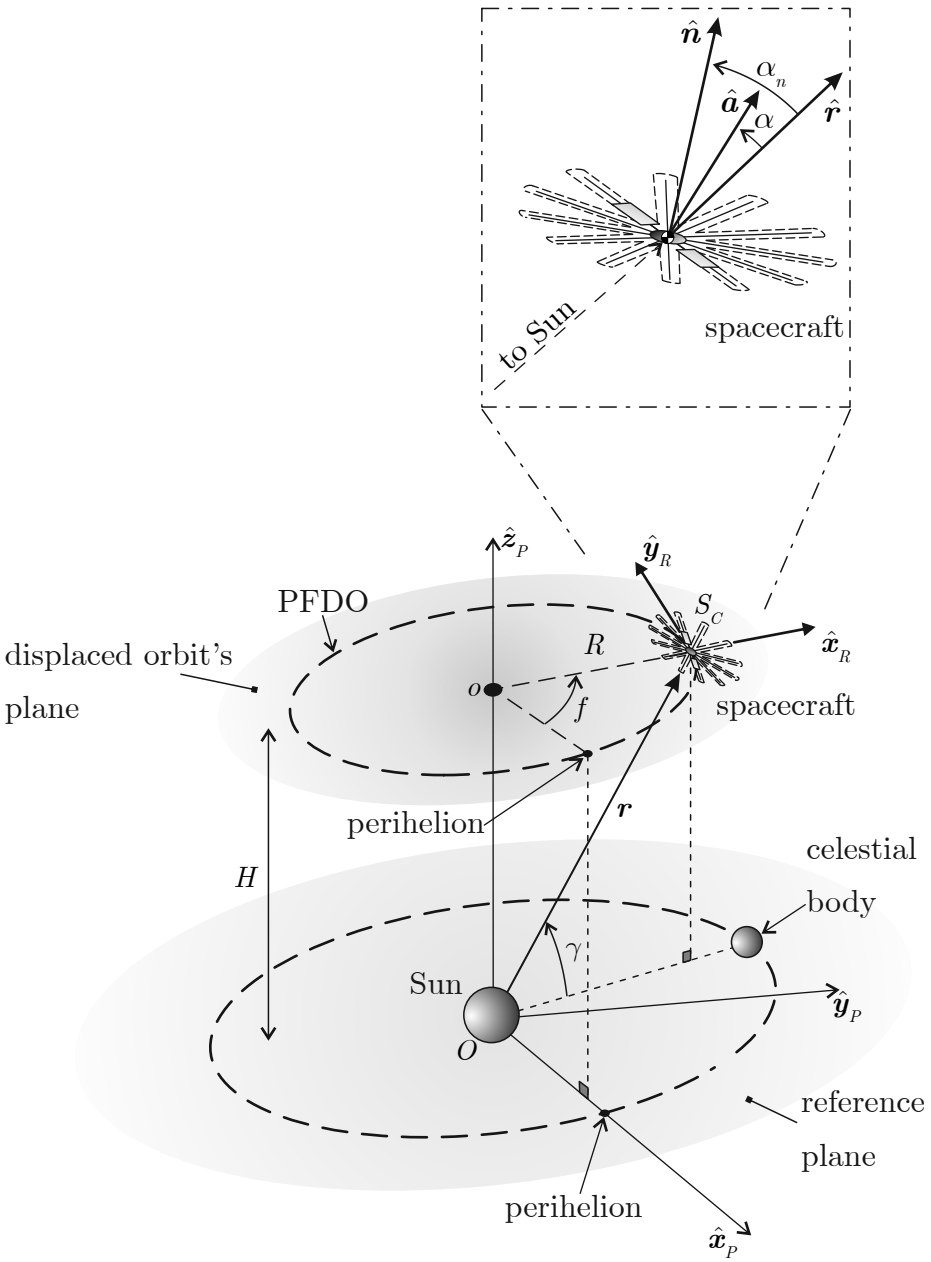

Figure 1: Reference frames and E-sail characteristic angles.

propulsive acceleration vector $\boldsymbol{a}$ is a function of both the Sun-spacecraft distance r, and the sail pitch angle $\alpha_n \in [0,\, 90]\,\mathrm{deg}$, the latter being the angle between the unit vector $\hat{\boldsymbol{n}}$ and the Sun-spacecraft unit vector $\hat{\boldsymbol{r}}$ (where $\hat{\boldsymbol{r}} \triangleq \boldsymbol{r}/r$, with $\boldsymbol{r}$ is the Sun-spacecraft position vector), viz.

$$\boldsymbol{a} = a_\oplus \left(\frac{r_\oplus}{r}\right) \kappa\, \hat{\boldsymbol{a}} \tag{1}$$

where $a_\oplus$ is the spacecraft characteristic acceleration, defined as the maximum modulus of $\boldsymbol{a}$ at a Sun-spacecraft reference distance $r_\oplus \triangleq 1\,\mathrm{au}$, whereas $\kappa = \kappa(\alpha_n) \in [0.5,\, 1]$ is the dimensionless propulsive

acceleration, defined as the ratio of the local value of $\|\boldsymbol{a}\|$ at a certain pitch angle α_n to the local maximum propulsive acceleration. Note that the value of $a_\oplus$ can be suitably varied along the spacecraft trajectory, by adjusting the tethers voltage [28, 29], to maintain an elliptic displaced orbit [30].

Since $\boldsymbol{a}$ belongs to the plane $(\hat{\boldsymbol{n}}, \hat{\boldsymbol{r}})$, the propulsive acceleration can be conveniently written as a function of the radial and normal unit vectors as [26]

$$\boldsymbol{a} = \begin{cases} a_\oplus \left(\dfrac{r_\oplus}{r}\right) \kappa \left[\dfrac{\sin(\alpha_n - \alpha)}{\sin\alpha_n}\,\hat{\boldsymbol{r}} + \dfrac{\sin\alpha}{\sin\alpha_n}\,\hat{\boldsymbol{n}}\right] & \text{if} \quad \alpha_n \in (0, \pi/2] \\ a_\oplus \left(\dfrac{r_\oplus}{r}\right) \hat{\boldsymbol{r}} & \text{if} \quad \alpha_n = 0 \end{cases} \tag{2}$$

where $\alpha = \alpha(\alpha_n) \in [0,\, 90]\,\text{deg}$ is the sail cone angle, i.e. the angle between the direction of $\hat{\boldsymbol{a}}$ and the Sun-spacecraft line. Bearing in mind the data given by [25], the variations of κ and α with the sail pitch angle α_n are shown in Fig. 2. Note that the cone angle reaches a maximum value of about 20 deg when $\alpha_n \simeq 55\,\text{deg}$, whereas the dimensionless propulsive acceleration is maximum ($\kappa = 1$) at $\alpha_n = 0$ (i.e., when $\hat{\boldsymbol{r}} \equiv \hat{\boldsymbol{n}}$ and the sail nominal plane is normal to the Sun-spacecraft line), and then decreases monotonically with α_n until $\kappa \simeq 0.5$. Further details about the thrust mathematical model for mission analysis purposes can be found in [26]. Also, a more accurate performance model could be obtained by taking into account the time delay associated with turning the tether rig.

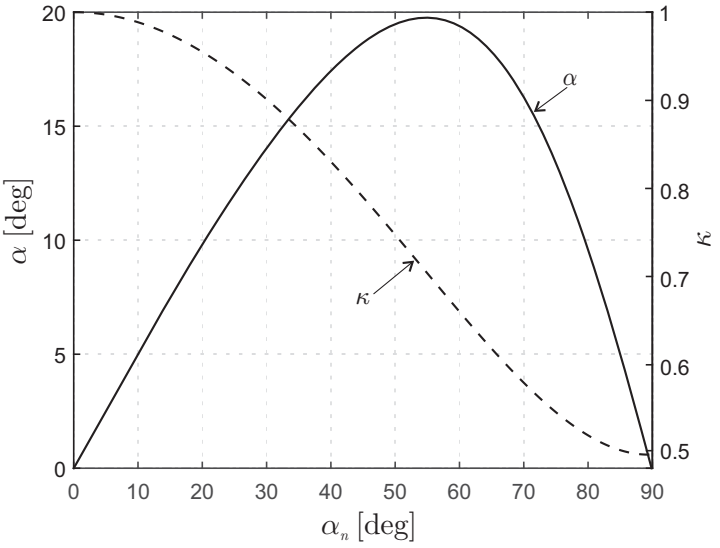

Figure 2: Sail cone angle α and dimensionless propulsive acceleration κ as a function of the sail pitch angle α_n.

2.2. Chief's elliptic displaced orbit

It is now useful to recall some mathematical relations that give an estimate of the propulsive performance necessary for maintaining a heliocentric, elliptic, displaced orbit using an E-sail propulsion system. For an in-depth discussion about this problem the interested reader is referred to [30, 31].

Consider a Keplerian, elliptic, reference orbit with a semimajor axis a_P and an eccentricity e_P. Without loss of generality, assume the nominal orbit to belong to the reference plane and introduce a heliocentric-perifocal frame $\mathcal{T}_P(O; \hat{\boldsymbol{x}}_P, \hat{\boldsymbol{y}}_P, \hat{\boldsymbol{z}}_P)$, see Fig. 1. For example, the nominal orbit could be the trajectory of a target celestial body (a planet or an asteroid) in a scientific observation mission. Note that the orbit of the celestial body is close to (but not necessarily in) the ecliptic plane due to a (small) inclination. A chief spacecraft (subscript C) is assumed to cover an elliptic displaced orbit, with semimajor axis a_C, eccentricity $e_C = e_P$, and whose orbital plane is parallel to that of the celestial body. With reference again to Fig. 1, introduce a rotating reference frame $\mathcal{T}_{R_C}(S_C; \hat{\boldsymbol{x}}_R, \hat{\boldsymbol{y}}_R, \hat{\boldsymbol{z}}_R)$, where $\hat{\boldsymbol{z}}_R$ axis is positive in the direction

of the spacecraft instantaneous angular velocity vector $\boldsymbol{\omega}$. The focus-pericenter direction of the displaced orbit is assumed to be parallel to the focus-pericenter direction of the reference orbit, whereas the chief's instantaneous angular velocity $\boldsymbol{\omega}_C$ matches the instantaneous angular velocity of the celestial body on the reference orbit. According to [30], such an orbit is referred to as Planet Following Displaced Orbit (PFDO).

The spacecraft equation of motion in the rotating frame $\mathcal{T}_{R_C}$ is

$$\ddot{\boldsymbol{r}}_C + 2\,\boldsymbol{\omega}_C \times \dot{\boldsymbol{r}}_C + \dot{\boldsymbol{\omega}}_C \times \boldsymbol{r}_C + \boldsymbol{\omega}_C \times (\boldsymbol{\omega}_C \times \boldsymbol{r}_C) = -\frac{\mu_\odot}{r_C^3}\,\boldsymbol{r}_C + \boldsymbol{a}_C \tag{3}$$

where $\boldsymbol{a}_C$ is the propulsive acceleration given by Eq. (2) as a function of the E-sail characteristics, and $\mu_\odot$ is the Sun's gravitational parameter. Note that $\boldsymbol{\omega}_C$ coincides, in this case, with the angular velocity of $\mathcal{T}_{R_C}$ with respect to $\mathcal{T}_P$. The components of the chief's position vector $\boldsymbol{r}_C$ in the frame $\mathcal{T}_{R_C}$ are

$$[\boldsymbol{r}_C]_{\mathcal{T}_{R_C}} = [R_C, \quad 0, \quad H_C]^{\mathrm{T}} \tag{4}$$

where H_C is the (constant) displaced orbit's plane distance with respect to the Sun's center-of-mass O, and R_C is the o-chief distance (i.e. the displaced orbit's focus-chief distance), see Fig. 1. For an elliptic displaced orbit, the distance R_C can be written as

$$R_C = \frac{a_C\,\left(1-e_C^2\right)}{1+e_C\,\cos f_C} \tag{5}$$

where f_C is the chief's true anomaly.

The components of Eq. (3) along the radial, circumferential and normal directions of the chief's rotating frame $\mathcal{T}_{R_C}$ are

$$\ddot{R}_C + \frac{\mu_\odot}{r_C^2}\,\cos\gamma_C - R_C\,\dot{f}_C^2 = a_\oplus\,\kappa_C\,\left(\frac{r_\oplus}{r_C}\right)\cos\left(\alpha_C+\gamma_C\right) \tag{6}$$

$$R_C\,\ddot{f}_C + 2\,\dot{R}_C\,\dot{f}_C = 0 \tag{7}$$

$$\frac{\mu_\odot}{r_C^2}\,\sin\gamma_C = a_\oplus\,\kappa_C\,\left(\frac{r_\oplus}{r_C}\right)\sin\left(\alpha_C+\gamma_C\right) \tag{8}$$

where γ_C is the chief's elevation angle defined as the angle between the Sun-spacecraft line and the orbital plane, viz.

$$\gamma_C = \arctan\left(\frac{H_C}{R_C}\right) \tag{9}$$

Since the chief's angular velocity $\dot{f}_C$ equals by assumption that of the reference celestial body $\|\boldsymbol{\omega}_C\|$, therefore [32]

$$\dot{f}_C = \|\boldsymbol{\omega}_C\| = \frac{n\,\left(1+e_C\,\cos f_C\right)^2}{\sqrt{\left(1-e_C^2\right)^3}} \tag{10}$$

where $n=\sqrt{\mu_\odot/a_P^3}$ is the mean motion along the reference celestial orbit. The term $\ddot{R}_C$ in Eq. (6) can be calculated from Eq. (5) as a function of $\{a_C,\,e_C,\,f_C\}$. In fact, taking into account Eq. (10), the result is

$$\ddot{R}_C = \frac{a_C\,e_C\,n^2}{\left(1-e_C^2\right)^2}\,\cos f_C\,\left(1+e_C\,\cos f_C\right)^2 \tag{11}$$

From Eq. (7), the component $h_{C_z} \triangleq \boldsymbol{h}_C \cdot \hat{\boldsymbol{z}}_{R_C}$ of the chief's specific angular momentum $\boldsymbol{h}_C$ along the $\hat{\boldsymbol{z}}_{R_C}$ axis is conservative, which implies

$$h_{C_z} = R_C^2\,\dot{f}_C = \text{constant} \tag{12}$$

The latter equation, taking into account Eqs. (5) and (10), gives

$$h_{C_z} = n\,a_C^2\,\sqrt{1-e_C^2} = \text{constant} \tag{13}$$

Substituting Eqs. (10)–(11) into Eqs. (8)–(7) and bearing in mind Eq. (13), the required cone angle α_C and characteristic acceleration $a_\oplus$ for maintaining a PFDO are obtained as a function of γ_C as

$$\tan\alpha_C = \frac{\xi_C^3\,\tan\gamma_C\,\sqrt{1+\tan^2\gamma_C}}{1-\xi_C^3\,\sqrt{1+\tan^2\gamma_C}} \tag{14}$$

$$\frac{a_\oplus}{\mu_\odot/r_\oplus^2} = \frac{r_\oplus}{\kappa_C\,H_C}\sqrt{\xi_C^6\,\tan^2\gamma_C\,\left(1+\tan^2\gamma_C\right) - 2\,\xi_C^3\,\frac{\tan^2\gamma_C}{\sqrt{1+\tan^2\gamma_C}} + \frac{\tan^2\gamma_C}{1+\tan^2\,\gamma_C}} \tag{15}$$

where

$$\xi_C \triangleq \frac{a_C}{a_P} \tag{16}$$

is the ratio between the semimajor axis of the (chief's) displaced and reference orbit. Equations (14)–(15) provide a compact formulation of the conditions necessary for maintaining a heliocentric, elliptic, displaced orbit using an E-sail propulsion system. These equations are valid for any elliptic displaced orbit and generalize the results discussed in [30], which are obtained using a different approach. Note that in the circular case (when $e_C = 0$), Eqs. (14)–(15) reduce to the results of [31].

The procedure for calculating the propulsive acceleration necessary for maintaining a given displaced orbit can now be summarized. First, choose the parameters of the reference Keplerian orbit $\{a_P,\, e_P\}$, and those of the displaced orbit to be reached $\{H_C,\, a_C\}$ (recall that $e_C = e_P$ by assumption). For a given point along the orbit characterized by f_C, calculate the value of R_C from Eq. (5), γ_C from Eq. (9), and the ratio ξ_C from Eq. (16). The cone angle α_C is obtained from Eq. (14). If α_C turns out to be greater than the maximum admissible value of about 20 deg, see Fig. 2, that means that the desired displaced orbit cannot be maintained by an E-sail. Otherwise, the dimensionless propulsive acceleration κ_C is derived from Fig. 2. Finally, the dimensionless value of the spacecraft characteristic acceleration is obtained from Eq. (15) (recall that $\mu_\odot/r_\oplus^2 \simeq 5.93\,\mathrm{mm/s^2}$).

3. Typical performance requirements

According to Eqs. (5) and (9), in the elliptic case the elevation angle γ_C varies as a function of the chief's true anomaly f_C. Therefore, the characteristic acceleration of the chief spacecraft $a_\oplus$ must be slightly modified along the trajectory to maintain the displaced orbit, and this can be achieved by suitably adjusting (within certain limits) the tether voltage [28, 29]. For a given value of the displaced orbit's semimajor axis a_C and displacement distance H_C, the maximum value of the required characteristic acceleration $a_{\oplus_{\max}} = \max(a_\oplus)$ is obtained when the chief is at its pericenter ($f_C = 0$), that is, when

$$\tan(\gamma_C) = \tan(\gamma_{C_{\max}}) \triangleq \frac{H_C}{a_C\,(1-e_C)} \equiv \frac{H_C}{\xi_C\,a_P\,(1-e_P)} \tag{17}$$

Moreover, according to Eq. (14), the cone angle takes its maximum value when $\gamma_C = \gamma_{C_{\max}}$ and, therefore, $f_C = 0$ is the most demanding condition in terms of propulsive requirements to meet.

Figure 3 illustrates the feasible regions and the contour lines of the maximum value of the spacecraft characteristic accelerations $a_{\oplus_{\max}}$ for some mission scenarios in which the reference celestial body is a planet. The figure clearly shows that, in all of the analyzed cases, the most favorable condition in terms of characteristic acceleration value it requires, is obtained when H_C is small and the semimajor axis a_C is near to that of the celestial body a_P. Note that for an observation mission, a spacecraft close to the planet is a good choice. However, in general, the spacecraft must avoid a close approach to the planet since the E-sail is unable to properly operate within the planetary magnetosphere that shields and deflects the solar wind. This same problem is, of course, much less important for other planets, such as Venus and Mars.

Taking into account the latter remark, Fig. 3 shows that the propulsive requirements for maintaining a displaced orbit tend to increase quickly with the displacement H_C, especially in the case of the inner planets. For example, if the reference celestial body is the Earth, a displaced orbit with $H_C = 0.05$ au and $a_C = 0.95$ au can be obtained using an E-sail with a maximum characteristic acceleration of about $1.16\,\mathrm{mm/s^2}$, see Fig. 3. That value corresponds to a medium-performance E-sail, whose technological level could be reached in the

near future [2]. However, with a characteristic acceleration of $1.16\,\mathrm{mm/s^2}$, a (relatively) small payload fraction can be obtained with the current technology level.

A potential solution to this problem is to distribute the payload among multiple E-sails in formation, with each sail being comprised of indispensable modules (e.g. communication and imaging module). In that way, the total mass of a single E-sail based spacecraft can be reduced and the propulsive performance, in terms of characteristic acceleration, can be improved. This is exactly the concept of disaggregated spacecraft, that is, to ideally split a monolithic spacecraft into multiple closely free-flying components that communicate with each other via inter-satellite links [16].

For example, using the mass breakdown model discussed by [15] and assuming a tether length of 15 km and a nominal tether voltage 25 kV, the value of the characteristic acceleration and the total spacecraft mass m can be calculated as a function of the payload mass m_{pay} and of the number of tethers N. The isocontour lines of the two functions $a_\oplus = a_\oplus(m_{\mathrm{pay}}, N)$ and $m = m(m_{\mathrm{pay}}, N)$ are drawn in Fig. 4. The figure shows that a given value of spacecraft characteristic acceleration can be obtained with different combinations of m_{pay} and N, thus obtaining different values of the total mass m. Under the assumption that the characteristic acceleration is set equal to the previous value of $1.16\,\mathrm{mm/s^2}$, it is possible to numerically calculate [15] the relation between the payload mass and the total spacecraft mass, see Fig. 5. From the figure, there is a linear relation between m and m_{pay} for a given $a_\oplus$. If, for example, $m_{\mathrm{pay}} = 200\,\mathrm{kg}$, the total spacecraft mass is about 750 kg. Assuming a maximum launch mass of 500 kg per spacecraft (for example, the payload capability of the 7300-series Delta II is about 600 kg for an interplanetary transfer orbit insertion), the payload could be (ideally) split up into two parts, each one with a mass of $1.15 \times 200/2 = 115\,\mathrm{kg}$, a value that includes a contingency factor of 15%. Accordingly, the mission could be accomplished using two spacecraft of 470 kg each (a value within the admissible range), operating in a formation flight.

Note that the reduction of the payload mass (for a given $a_\oplus$) also implies a substantial simplification in the E-sail propulsion system as the required number of tethers decreases. In fact, Fig. 6 shows that if $m_{\mathrm{pay}} = 200\,\mathrm{kg}$, a characteristic acceleration of $1.16\,\mathrm{mm/s^2}$ may be obtained using about 100 tethers. If, instead, $m_{\mathrm{pay}} = 115\,\mathrm{kg}$, the number of tethers decreases to 60. Since the length of each tether is by assumption equal to 15 km, a reduction of N implies a reduction of the total tether length and a corresponding simplification of the propulsion system.

4. Geometrical analysis of formation flying

Having analyzed the generation of an elliptic displaced orbit for the chief spacecraft from the point of view of the required propulsive performance, we are now in a position to study the relative motion of two E-sail based spacecraft, the chief and the deputy (subscript D), moving along two different displaced orbits. In particular, the deputy tracks a heliocentric displaced orbit whose orbital parameters are slightly different from that of the chief spacecraft.

It has been pointed out by [22] that when the semimajor axis and eccentricity of the two displaced orbits are given, the relative motion between the two spacecraft is univocally established, and evolves on its invariant manifold. In the discussion to follow, the geometry and bounds of the formation will be analyzed in the configuration space using a purely geometric approach, taking into account the recent results of [23].

4.1. Approximate form of relative motion equations

Let $\boldsymbol{\rho} \triangleq \boldsymbol{r}_D - \boldsymbol{r}_C$ denote the relative position vector between the two spacecraft, where $\boldsymbol{r}_D$ is the Sun-deputy vector, and introduce a rotating reference frame $\mathcal{T}_{R_D}(S_D; \hat{\boldsymbol{x}}_{R_D}, \hat{\boldsymbol{y}}_{R_D}, \hat{\boldsymbol{z}}_{R_D})$, involving the deputy spacecraft, defined in a perfectly similar way as that of the chief. According to [23], the components of $\boldsymbol{\rho}$ in the chief's rotating reference frame $\mathcal{T}_{R_C}$ can be written as

$$[\boldsymbol{\rho}]_{\mathcal{T}_{R_C}} = \mathbb{T}^{\mathrm{T}}_{R_C I}\left(\Omega_C, i_C, \theta_C\right)\, \mathbb{T}_{R_D I}\left(\Omega_D, i_D, \theta_D\right)\, [\boldsymbol{r}_D]_{\mathcal{T}_{R_D}} - [\boldsymbol{r}_C]_{\mathcal{T}_{R_C}} \tag{18}$$

where Ω is the right ascension of the ascending node, i is the inclination and $\theta = \varpi + f$ is the argument of latitude. The three angles $\{\Omega, i, \varpi\}$, which define the orientation of the displaced orbit with respect to the inertial frame $\mathcal{T}_I$, closely resemble the classical definition used for Keplerian orbits, as is discussed by [23].

The transformation matrix $\mathbb{T}_{RI}$ from $\mathcal{T}_R$ to $\mathcal{T}_I$, written as a function of the three Euler's angles $\{\Omega, i, \theta\}$, is given by

$$\mathbb{T}_{RI}\ (\Omega, i, \theta) \triangleq \begin{bmatrix} (\cos\theta\ \cos\Omega - \sin\theta\ \cos i\ \sin\Omega) & (-\sin\theta\ \cos\Omega - \cos\theta\ \cos i\ \sin\Omega) & (\sin i\ \sin\Omega) \\ (\cos\theta\ \sin\Omega + \sin\theta\ \cos i\ \cos\Omega) & (-\sin\theta\ \sin\Omega + \cos\theta\ \cos i\ \cos\Omega) & (-\sin i\ \cos\Omega) \\ \sin\theta\ \sin i & \cos\theta\ \sin i & \cos i \end{bmatrix} \tag{19}$$

For the sake of brevity, the following shorthand notation is now introduced

$$\mathbb{T}_{R_D R_C} \triangleq \mathbb{T}^{\mathrm{T}}_{R_C I}\left(\Omega_C, i_C, \theta_C\right)\ \mathbb{T}_{R_D I}\left(\Omega_D, i_D, \theta_D\right) \tag{20}$$

where $\mathbb{T}_{R_D R_C}$ (with generic entry T_{ij}) represents the transformation matrix between the two rotating frames (from $\mathcal{T}_{R_D}$ to $\mathcal{T}_{R_C}$).

Assume that the chief and deputy fly close to each other. Accordingly, the relative orbital elements of the two spacecraft are first-order small quantities, that is, $\Delta\theta \triangleq \theta_D - \theta_C \ll 1$, $\Delta\Omega \triangleq \Omega_D - \Omega_C \ll 1$, and $\Delta i \triangleq i_D - i_C \ll 1$. Therefore, the entries T_{ij} of the transformation matrix $\mathbb{T}_{R_D R_C}$ can be approximated as

$$\begin{aligned} T_{11} = T_{22} = T_{33} \simeq 1, \quad T_{12} = -T_{21} \simeq \left(\Delta\theta + \cos\ i_C\ \Delta\Omega\right), \\ T_{13} = -T_{31} \simeq \cos\ i_C\ \cos\ \theta_C\ \Delta\Omega - \sin\theta_C\ \Delta i, \\ T_{23} = -T_{32} \simeq -\left(\cos\ i_C\ \sin\theta_C\ \Delta\Omega + \cos\ \theta_C\ \Delta i\right) \end{aligned} \tag{21}$$

Substituting Eqs. (20)–(21) in Eq. (18), the radial, along-track and normal components of the relative position vector $\boldsymbol{\rho}$ can be expressed in the chief's rotating frame $\mathcal{T}_{R_C}$ as

$$\rho_x \simeq \Delta R + H_C\ \left(\sin i_C\ \cos\theta_C\ \Delta\Omega - \sin\theta_C\ \Delta i\right) \tag{22}$$

$$\rho_y \simeq R_C\ \left(\Delta\theta + \cos i_C\ \Delta\Omega\right) - H_C\ \left(\sin i_C\ \sin\theta_C\ \Delta\Omega + \cos\theta_C\ \Delta i\right) \tag{23}$$

$$\rho_z \simeq R_C\ \left(\sin\theta_C\ \Delta i - \sin i_C\ \cos\theta_C\ \Delta\Omega\right) + \Delta H \tag{24}$$

where $\Delta R \triangleq R_D - R_C$ and $\Delta H \triangleq H_D - H_C$. Note that, enforcing the condition $H_C = H_D = 0$, Eqs. (22)–(24) reduce to a form consistent with the Keplerian case [33, 34, 35].

If the relative distance between the two spacecraft is sufficiently small, the term ΔR may be approximated using its differential, that is

$$\Delta R = \left.\frac{\partial R}{\partial a}\right|_C \Delta a + \left.\frac{\partial R}{\partial e}\right|_C \Delta e + \left.\frac{\partial R}{\partial f}\right|_C \Delta f \tag{25}$$

with

$$\left.\frac{\partial R}{\partial a}\right|_C \equiv \frac{\partial R_C}{\partial a_C} = \frac{1 - e_C^2}{1 + e_C\ \cos f_C} \tag{26}$$

$$\left.\frac{\partial R}{\partial e}\right|_C \equiv \frac{\partial R_C}{\partial e_C} = -\frac{a_C\ \left[2\, e_C + \left(1 + e_C^2\right)\ \cos f_C\right]}{\left(1 + e_C\ \cos f_C\right)^2} \tag{27}$$

$$\left.\frac{\partial R}{\partial f}\right|_C \equiv \frac{\partial R_C}{\partial f_C} = \frac{a_C\, e_C\ \left(1 - e_C^2\right)\ \sin f_C}{\left(1 + e_C\ \cos f_C\right)^2} \tag{28}$$

where the expression of R_C given by Eq. (5) has been considered. Using the relation between the true anomaly f and the mean anomaly M, it can be verified that [33]

$$\Delta f = \frac{\left(1 + e_C\ \cos f_C\right)^2}{\sqrt{\left(1 - e_C^2\right)^3}}\ \Delta M + \frac{\left(2 + e_C\ \cos f_C\right)\ \sin f_C}{1 - e_C^2}\ \Delta e \tag{29}$$

where $\Delta M \triangleq M_D - M_C$ and $\Delta e \triangleq e_D - e_C$.

For a formation flight mission, the two spacecraft should satisfy the periodic (or 1:1 commensurability) condition, otherwise the relative motion would be locally unbounded. The mean motion of the two spacecraft must take the same value, i.e. $n_C = n_D$. Note that $M = M_0 + n\,(t - t_0)$, therefore the periodic condition implies $\Delta M = \Delta M_0$. The parametric solution to spacecraft relative motion can be obtained in terms of displaced orbital elements differences by substituting Eqs. (25)–(29) into Eqs. (22)–(24). Using the chief's true anomaly f_C as the independent variable, the solution can be written as

$$\rho_x \simeq \frac{1-e_C^2}{1+e_C\,\cos\,f_C}\,\Delta a - a_C\,\cos\,f_C\,\Delta e - H_C\,\sin\left(\varpi_C + f_C\right)\,\Delta i$$
$$+ H_C\,\sin i_C\,\cos\,\left(\varpi_C + f_C\right)\,\Delta\Omega + \frac{a_C\,e_C\,\sin f_C}{\sqrt{1-e_C^2}}\,\Delta M_0 \tag{30}$$

$$\rho_y \simeq \frac{a_C\,\left(2 + e_C\,\cos\,f_C\right)\,\sin f_C}{1+e_C\,\cos\,f_C}\,\Delta e + \left[\frac{a_C\,\left(1-e_C^2\right)\,\cos\,i_C}{1+e_C\,\cos\,f_C} - H_C\,\sin i_C\,\sin\left(\varpi_C + f_C\right)\right]\Delta\Omega$$
$$+ \frac{a_C\,\left(1-e_C^2\right)}{1+e_C\,\cos\,f_C}\,\Delta\varpi + \frac{a_C\,\left(1+e_C\,\cos\,f_C\right)}{\sqrt{1-e_C^2}}\,\Delta M_0 \tag{31}$$

$$\rho_z \simeq \frac{a_C\,\left(1-e_C^2\right)}{1+e_C\,\cos\,f_C}\,\sin\left(\varpi_C + f_C\right)\Delta i - \frac{a_C\,\left(1-e_C^2\right)}{1+e_C\,\cos\,f_C}\,\cos\left(\varpi_C + f_C\right)\,\sin i_C\,\Delta\Omega + \Delta H \tag{32}$$

Observe that the only assumption made so far to linearize the relative motion equations is that the relative (displaced) orbital elements of the two spacecraft are small quantities. In a general case with two highly elliptic displaced orbits, the relative motion geometry represented by Eqs. (30)–(32) is very complex, and the invariant manifold along which it evolves resembles a quadric or a quartic surface [22, 23]. However, if the eccentricity of the chief's orbit is sufficiently small, i.e. if $e_C \ll 1$, an interesting (simplified) form of relative motion equations can be obtained with the following approximations

$$\frac{1}{1+e_C\,\cos f_C} \simeq 1 - e_C\,\cos\,f_C \qquad \text{and} \qquad \sqrt{1-e_C^2} \simeq 1 \tag{33}$$

In fact, substituting Eq. (33) into Eqs. (30)–(32), the first-order approximation of the components of relative position vector becomes

$$\rho_x \simeq \Delta a + \left(-e_C\,\Delta a - a_C\,\Delta e - H_C\,\sin\varpi_C\,\Delta i + H_C\,\sin i_C\,\cos\varpi_C\,\Delta\Omega\right)\cos f_C$$
$$+ \left(-H_C\,\cos\varpi_C\,\Delta i - H_C\,\sin i_C\,\sin\varpi_C\,\Delta\Omega + a_C\,e_C\,\Delta M_0\right)\sin f_C \tag{34}$$

$$\rho_y \simeq a_C\,\left(\cos i_C\,\Delta\Omega + \Delta\varpi + \Delta M_0\right)$$
$$+ \left[a_C\,e_C\,\left(\Delta M_0 - \cos i_C\,\Delta\Omega - \Delta\varpi\right) - H_C\,\left(\cos\varpi_C\,\Delta i + \sin i_C\,\sin\varpi_C\,\Delta\Omega\right)\right]\,\cos\,f_C$$
$$+ \left[2\,a_C\,\Delta e + H_C\,\left(\sin\varpi_C\,\Delta i - \sin i_C\,\cos\varpi_C\,\Delta\Omega\right)\right]\,\sin f_C - a_C\,e_C\,\Delta e\,\sin 2f_C \tag{35}$$

$$\rho_z \simeq \frac{1}{2}\,a_C\,e_C\,\left(\sin i_C\,\cos\varpi_C\,\Delta\Omega - \sin\varpi_C\,\Delta i + \Delta H\right) + a_C\,\left(\sin\varpi_C\,\Delta i - \sin i_C\,\cos\varpi_C\,\Delta\Omega\right)\,\cos f_C$$
$$+ a_C\,\left(\cos\varpi_C\,\Delta i + \sin i_C\,\sin\varpi_C\,\Delta\Omega\right)\,\sin f_C + \frac{1}{2}\,a_C\,e_C\,\left(\sin i_C\,\cos\varpi_C\,\Delta\Omega - \sin\varpi_C\,\Delta i\right)\,\cos 2f_C$$
$$- \frac{1}{2}\,a_C\,e_C\,\left(\cos\varpi_C\,\Delta i + \sin i_C\,\sin\varpi_C\,\Delta\Omega\right)\,\sin 2f_C \tag{36}$$

In particular, if the chief spacecraft tracks a circular displaced orbit, i.e. when $e_C = 0$, Eqs. (34)–(36) reduce to the compact form

$$\rho_x \simeq \Delta a + A_x \, \sin\left(f_C + \varphi_x\right) \tag{37}$$

$$\rho_y \simeq a_C \, \left(\cos i_C \, \Delta\Omega + \Delta\varpi + \Delta M_0\right) + A_y \, \sin\left(f_C + \varphi_y\right) \tag{38}$$

$$\rho_z \simeq \Delta H + A_z \, \sin\left(f_C + \varphi_z\right) \tag{39}$$

where

$$A_x = \sqrt{a_C^2 \, \Delta e^2 + 2\, a_C \, H_C \, \Delta e \, \left(\sin\varpi_C \, \Delta i - \sin i_C \, \cos\varpi_C \, \Delta\Omega\right) + H_C^2 \, \left(\Delta i^2 + \sin^2 i_C \, \Delta\Omega^2\right)} \tag{40}$$

$$A_y = \sqrt{4\, a_C^2 \, \Delta e^2 + 4\, a_C \, H_C \, \Delta e \, \left(\sin\varpi_C \, \Delta i - \sin i_C \, \cos\varpi_C \, \Delta\Omega\right) + H_C^2 \, \left(\Delta i^2 + \sin^2 i_C \, \Delta\Omega^2\right)} \tag{41}$$

$$A_z = a_C \, \sqrt{\Delta i^2 + \sin^2 i_C \, \Delta\Omega^2} \tag{42}$$

$$\varphi_x = \arctan\left[\frac{H_C \, \left(\sin\varpi_C \, \Delta i - \sin i_C \, \cos\varpi_C \, \Delta\Omega\right) + a_C \, \Delta e}{H_C \, \left(\cos\varpi_C \, \Delta i + \sin i_C \, \sin\varpi_C \, \Delta\Omega\right)}\right] \tag{43}$$

$$\varphi_y = \arctan\left[\frac{H_C \, \left(\cos\varpi_C \, \Delta i + \sin i_C \, \sin\varpi_C \, \Delta\Omega\right)}{H_C \, \left(\sin i_C \, \cos\varpi_C \, \Delta\Omega - \sin\varpi_C \, \Delta i\right) - 2\, a_C \, \Delta e}\right] \tag{44}$$

$$\varphi_z = \arctan\left[\frac{\sin\varpi_C \, \Delta i - \sin i_C \, \cos\varpi_C \, \Delta\Omega}{\cos\varpi_C \, \Delta i + \sin i_C \, \sin\varpi_C \, \Delta\Omega}\right] \tag{45}$$

Equations (37)–(39) constitute a parametric representation of an elliptic cylinder, which can be considered a degenerated manifold of the full relative motion problem. Note that if $\Delta e = 0$ and $H_C \neq 0$, the in-plane projection of the relative motion is a circle with a radius $A_x = A_y = H_C \, \sqrt{\Delta i^2 + \sin^2 i_C \, \Delta\Omega^2}$. The other special case happens when $\Delta e \neq 0$ and $H_C = 0$. In this case $A_x/A_y = 1/2$, which corresponds to an in-plane projected ellipse with a semimajor axis equal to $2\, a_C \, \Delta e$ and a semiminor axis equal to $a_C \, \Delta e$.

4.2. Bounds of relative motion

An essential prerequisite for a formation flight is that the relative distance of the two spacecraft be confined within a well-defined region with some (assigned) lower and upper bounds. These bounds play a fundamental role in establishing the size of the formation. Unlike previous studies [23] in which these values were calculated by solving some high-order (either quartic or sextic) equations, in this paper they are obtained in an explicit form as a function of the displaced orbital elements.

To this end, introduce the substitution $s \triangleq \tan(f_C/2)$ and assume a small eccentricity of the chief's orbit. It can be verified that the generic solution of the relative motion described by Eqs. (30)–(32) can be approximated as

$$\rho_x \simeq \lambda_1 + 2 \, \frac{\lambda_2 \, s + \lambda_3}{s^2 + 1} \tag{46}$$

$$\rho_y \simeq \lambda_4 + 2 \, \frac{\lambda_5 \, s + \lambda_6}{s^2 + 1} \tag{47}$$

$$\rho_z \simeq \lambda_7 + 2 \, \frac{\lambda_8 \, s + \lambda_9}{s^2 + 1} \tag{48}$$

where the coefficients $\lambda_1, \lambda_2, \ldots, \lambda_9$ are

$$\lambda_1 = (1 + e_C)\ \Delta a + a_C\, \Delta e + H_C\, \sin\varpi_C\, \Delta i - H_C\, \sin i_C\, \cos\varpi_C\, \Delta\Omega \tag{49}$$

$$\lambda_2 = -H_C\, \cos\varpi_C\, \Delta i - H_C\, \sin i_C\, \sin\varpi_C\, \Delta\Omega + a_C\, e_C\, \Delta M_0 \tag{50}$$

$$\lambda_3 = -e_C\, \Delta a - a_C\, \Delta e - H_C\, \sin\varpi_C\, \Delta i + H_C\, \sin i_C\, \cos\varpi_C\, \Delta\Omega \tag{51}$$

$$\begin{aligned}\lambda_4 = {} & H_C\, \cos\varpi_C\, \Delta i + [a_C\, (1 + e_C)\, \cos i_C + H_C\, \sin i_C\, \sin\varpi_C]\ \Delta\Omega \\ & + a_C\, (1 + e_C)\ \Delta\varpi + a_C\, (1 - e_C)\ \Delta M_0\end{aligned} \tag{52}$$

$$\lambda_5 = a_C\, (2 + e_C)\ \Delta e + H_C\, \sin\varpi_C\, \Delta i - H_C\, \sin i_C\, \cos\varpi_C\, \Delta\Omega \tag{53}$$

$$\begin{aligned}\lambda_6 = {} & -H_C\, \cos\varpi_C\, \Delta i - [a_C\, e_C\, (1 + e_C)\, \cos i_C + H_C\, \sin i_C\, \sin\varpi_C]\ \Delta\Omega \\ & - a_C\, e_C\, (1 + e_C)\ \Delta\varpi + a_C\, e_C\, \Delta M_0\end{aligned} \tag{54}$$

$$\lambda_7 = -a_C\, (1 + e_C)\, \sin\varpi_C\, \Delta i + a_C\, (1 + e_C)\, \sin i_C\, \cos\varpi_C\, \Delta\Omega + \Delta H \tag{55}$$

$$\lambda_8 = a_C\, (1 + e_C\,)\, \cos\varpi_C\, \Delta i + a_C\, (1 + e_C)\, \sin i_C\, \sin\varpi_C\, \Delta\Omega \tag{56}$$

$$\lambda_9 = a_C\, (1 + 2\, e_C) + H_C\, \sin\varpi_C\, \Delta i - H_C\, \sin i_C\, \cos\varpi_C\, \Delta\Omega \tag{57}$$

In general, the relative motion is three dimensional and always evolves on its invariant manifold. However, under the assumption $e_C \ll 1$, as per Eqs. (46)–(48), the relative motion lies on a plane parameterized by

$$C_x\, \rho_x + C_y\, \rho_y + C_z\, \rho_z + C_0 = 0 \tag{58}$$

where

$$C_x = \lambda_5\, \lambda_9 - \lambda_6\, \lambda_8 \tag{59}$$

$$C_y = \lambda_3\, \lambda_8 - \lambda_2\, \lambda_9 \tag{60}$$

$$C_z = \lambda_2\, \lambda_6 - \lambda_3\, \lambda_5 \tag{61}$$

$$C_0 = \lambda_1\, \lambda_6\, \lambda_8 - \lambda_1\, \lambda_5\, \lambda_9 + \lambda_2\, \lambda_4\, \lambda_9 - \lambda_3\, \lambda_4\, \lambda_8 + \lambda_3\, \lambda_5\, \lambda_7 - \lambda_2\, \lambda_6\, \lambda_7 \tag{62}$$

The bounds for each component of the relative position vector can be found by enforcing the necessary conditions

$$\frac{\partial\, \rho_i}{\partial\, s} = 0 \quad \text{with} \quad i = \{x, y, z\} \tag{63}$$

where the components ρ_i are given by Eqs. (46)–(48). From Eq. (63), the critical values of s corresponding to the radial bounds (denoted with the superscript $\star$) are obtained as

$$s_x^\star = \frac{-\lambda_3 \pm \sqrt{\lambda_2^2 + \lambda_3^2}}{\lambda_2} \tag{64}$$

and the maximum and minimum radial distances are

$$\rho_x^\star = \lambda_1 + \lambda_3 \pm \sqrt{\lambda_2^2 + \lambda_3^2} \tag{65}$$

Note that the mapping from f to s introduces a number of inherent singularities $s = \pm\infty$ at $f = k\,\pi$ (where $k \in \mathbb{N}$), which occur when $\lambda_2 = 0$. In these cases, the extreme values are identical, that is, $\rho_{x_{\max}} = \rho_{x_{\min}} = \lambda_1$.

Likewise, for the along-track and normal motion, the critical values of s and the corresponding extreme values of distances bounds are

$$s_y^\star = \frac{-\lambda_6 \pm \sqrt{\lambda_5^2 + \lambda_6^2}}{\lambda_5} \tag{66}$$

$$\rho_y^\star = \lambda_4 + \lambda_6 \pm \sqrt{\lambda_5^2 + \lambda_6^2} \tag{67}$$

$$s_z^\star = \frac{-\lambda_9 \pm \sqrt{\lambda_8^2 + \lambda_9^2}}{\lambda_8} \tag{68}$$

$$\rho_z^\star = \lambda_7 + \lambda_9 \pm \sqrt{\lambda_8^2 + \lambda_9^2} \tag{69}$$

The singularities corresponding to $\lambda_5 = 0$ or $\lambda_8 = 0$ take place when $f = k\,\pi$. In these special cases, the extreme values for the along-track and normal motion reduce to $\rho_{y_{\max}} = \rho_{y_{\min}} = \lambda_4$ and $\rho_{z_{\max}} = \rho_{z_{\min}} = \lambda_7$, respectively.

The relative distance bounds of the two spacecraft can also be found using Eqs. (46)–(48). Let $\rho \triangleq \|\boldsymbol{\rho}\| = \sqrt{\rho_x^2 + \rho_y^2 + \rho_z^2}$ be the two spacecraft relative distance, then

$$\rho^2 = \eta + \frac{\sigma_3\, s^3 + \sigma_2\, s^2 + \sigma_1\, s + \sigma_0}{\left(s^2 + 1\right)^2} \tag{70}$$

where

$$\sigma_0 = 4\left(\lambda_1\,\lambda_3 + \lambda_4\,\lambda_6 + \lambda_7\,\lambda_9 + \lambda_3^2 + \lambda_6^2 + \lambda_9^2\right) \tag{71}$$

$$\sigma_1 = 4\left(\lambda_1\,\lambda_2 + \lambda_4\,\lambda_5 + \lambda_7\,\lambda_8 + 2\,\lambda_2\,\lambda_3 + 2\,\lambda_5\,\lambda_6 + 2\,\lambda_8\,\lambda_9\right) \tag{72}$$

$$\sigma_2 = 4\left(\lambda_1\,\lambda_3 + \lambda_4\,\lambda_6 + \lambda_7\,\lambda_9 + \lambda_2^2 + \lambda_5^2 + \lambda_8^2\right) \tag{73}$$

$$\sigma_3 = 4\left(\lambda_1\,\lambda_2 + \lambda_4\,\lambda_5 + \lambda_7\,\lambda_8\right) \tag{74}$$

$$\eta = \lambda_1^2 + \lambda_4^2 + \lambda_7^2 \tag{75}$$

The condition to be met for obtaining the extreme values of the relative distance is

$$\frac{\partial(\rho^2)}{\partial\, s} = 0 \tag{76}$$

which amounts to solving a quartic equation in the variable s given by.

$$\sigma_3\, s^4 + 2\,\sigma_2\, s^3 + 3\,\left(\sigma_1 - \sigma_3\right)\, s^2 + 2\,\left(\sigma_2 - 2\,\sigma_0\right)\, s + \sigma_1 = 0 \tag{77}$$

whose real roots can be easily found numerically using a standard approach.

5. Case study

To verify the proposed methodology for analyzing the formation geometry and the distance bounds of relative motion between two E-sail based spacecraft, Eq. (18) is now assumed as the reference solution and is compared with the (approximate) analytical results. The Earth is taken as the reference celestial body with a semimajor axis $a_P = 1\,\text{au}$ and an eccentricity $e_P = 0.0167$, with the chief spacecraft covering a PFDO. The deputy's orbital elements are slightly different from those of the chief and, in order to guarantee the periodicity of relative motion, the mean motions of the two spacecraft are assumed $n_C = n_D = \sqrt{\mu_\odot/(1\,\text{au})^3}$,

	a [au]	H [au]	e	i [deg]	Ω [deg]	ϖ [deg]	f_0 [deg]
chief	0.95	0.05	0.0167	0.001	224	237	0
deputy	0.925	0.051	0.01	1	225	238	0

Table 1: Characteristics of the two PFDOs considered in the simulations.

a value that coincides with the Earth's mean motion. The relevant data of the two PFDOs are summarized in Tab. 1.

The required characteristic accelerations necessary to maintain the displaced orbits as a function of the true anomaly for the two spacecraft are shown in Fig. 7, while the variations of the chief and deputy's pitch angles are illustrated in Fig. 8. Figure 9 depicts the formation geometry obtained from the approximate solution of Eqs. (30)–(32), which fits well the reference numerical results, as is clearly shown in Fig. 10.

The extreme values of relative distances, as well as the critical values of the chief's true anomaly, are summarized in Tab. 2. The performance of the parametric representation of Eqs. (46)–(48) is illustrated in Fig. 11, indicating how the approximate extreme values are able to successfully predict the lower and upper bounds of the relative distances.

Component	$s^\star$		$f_C^\star \bmod 360\,[\,\mathrm{deg}]$		Extreme values	
ρ_x	3.1507×10^{-2}	-3.1739×10^{1}	3.6092	1.8361×10^{2}	-1.7443×10^{-2}	-3.2529×10^{-2}
ρ_y	-1.0072	9.9282×10^{-1}	2.6959×10^{2}	8.9587×10^{1}	4.6712×10^{-2}	1.95728×10^{-2}
ρ_z	-3.4240	2.9206×10^{-1}	2.1256×10^{2}	3.2562×10^{1}	1.7802×10^{-2}	-1.6282×10^{-2}
ρ	-1.6213	1.0635	2.4333×10^{2}	9.3525×10^{1}	5.5850×10^{-2}	3.2627×10^{-2}

Table 2: Extreme values of the relative distances bounds.

In principle, the accuracy of the approximate solution relies on the differences of the orbital elements and the eccentricity of the chief (which is small by assumption). To better emphasize the importance of e_C, Fig. 12 shows the accuracy level that can be obtained by varying the chief's orbital eccentricity in a range $e_C \in [0, 0.1]$, while maintaining unchanged the other parameters of Tab. 1. Note that the accuracy decreases with e_C, but the approximate solution still performs well until $e_C \leq 0.04$. The accuracy level is better illustrated in Fig. 13, which quantifies the maximum error along a full orbit using the approximate solution. Note that the minimum value of the maximum error is approximately obtained when $e_C = e_D = 0.0167$, that is, when the relative eccentricity (Δe) tends to zero.

6. Conclusions

The feasibility of maintaining an elliptic displaced orbit using an E-sail has been investigated using a geometrical approach. The problem of studying the formation flying between two E-sail based spacecraft that cover displaced orbits has been parameterized by a set of displaced orbital elements using a semi-analytical procedure. Assuming a small difference in the orbital elements, the closed-form solution to the relative motion can be described in an algebraic form via relative orbital elements.

In particular, in the case of small eccentricity, the extreme values for the relative distances can be calculated analytically through the solution of an algebraic equation. This result is useful for determining the formation boundaries with a given set of orbital elements or to estimate the reachable domain when some uncertainties exist in the orbital elements. However, maintaining the formation requires an active control strategy where, in general, both the characteristic acceleration and the sail attitudes vary as a function of the spacecraft relative distance. The control strategy is closely related to the formation structure, as is discussed in the companion paper [27].

7. Acknowledgements

This work was funded by the National Natural Science Foundation of China (No. 11472213) and Open Research Foundation of Science and Technology in Aerospace Flight Dynamics Laboratory of China (No. 2015afdl016). This work was also supported by the Chinese Scholarship Council.

References

[1] P. Janhunen, A. Sandroos, Simulation study of solar wind push on a charged wire: basis of solar wind electric sail propulsion, Annales Geophysicae 25 (3) (2007) 755–767, doi: 10.5194/angeo-25-755-2007.

[2] P. Janhunen, P. K. Toivanen, J. Polkko, S. Merikallio, P. Salminen, E. Haeggstrom, H. Seppanen, R. Kurppa, J. Ukkonen, S. Kiprich, G. Thornell, H. Kratz, L. Richter, O. Kromer, R. Rosta, M. Noorma, J. Envall, S. Latt, G. Mengali, A. A. Quarta, H. Koivisto, O. Tarvainen, T. Kalvas, J. Kauppinen, A. Nuottajarvi, A. Obraztsov, Electric solar wind sail: Towards test missions, Review of Scientific Instruments 81 (11) (2010) 111301 (1–11), doi: 10.1063/1.3514548.

[3] A. Sanchez-Torres, Drag and propulsive forces in electric sails with negative polarity, Advances in Space Research 57 (4) (2016) 1065–1071, doi: 10.1016/j.asr.2015.12.013.

[4] A. A. Quarta, G. Mengali, Electric sail missions to potentially hazardous asteroids, Acta Astronautica 66 (9-10) (2010) 1506–1519, doi: 10.1016/j.actaastro.2009.11.021.

[5] G. Mengali, A. A. Quarta, G. Aliasi, A graphical approach to electric sail mission design with radial thrust, Acta Astronautica 82 (2) (2013) 197–208, doi: 10.1016/j.actaastro.2012.03.022.

[6] K. Yamaguchi, H. Yamakawa, Electric solar wind sail kinetic energy impactor for asteroid deflection missions, The Journal of the Astronautical Sciences 63 (1) (2016) 1–22, doi: 10.1007/s40295-015-0081-x.

[7] G. Mengali, A. A. Quarta, P. Janhunen, Electric sail performance analysis, Journal of Spacecraft and Rockets 45 (1) (2008) 122–129, doi: 10.2514/1.31769.

[8] A. A. Quarta, G. Mengali, P. Janhunen, Optimal interplanetary rendezvous combining electric sail and high thrust propulsion system, Acta Astronautica 68 (5-6) (2011) 603–621, doi: 10.1016/j.actaastro.2010.01.024.

[9] R. J. McKay, M. Macdonald, J. Biggs, C. R. McInnes, Survey of highly-non-Keplerian orbits with low-thrust propulsion, Journal of Guidance, Control, and Dynamics 34 (3) (2011) 645–666, doi: 10.2514/1.52133.

[10] F. Salazar, C. McInnes, O. Winter, Intervening in earth's climate system through space-based solar reflectors, Advances in Space Research 58 (1) (2016) 17–29, doi: 10.1016/j.asr.2016.04.007.

[11] T. J. Waters, C. R. McInnes, Periodic orbits above the ecliptic in the solar-sail restricted three-body problem, Journal of Guidance, Control and Dynamics 30 (3) (2007) 687–693, doi: 10.2514/1.26232.

[12] G. Mengali, A. A. Quarta, Non-Keplerian orbits for electric sails, Celestial Mechanics and Dynamical Astronomy 105 (1–3) (2009) 179–195, doi: 10.1007/s10569-009-9200-y.

[13] C. R. McInnes, J. F. L. Simmons, Solar sail halo orbits I: Heliocentric case, Journal of Spacecraft and Rockets 29 (4) (1992) 466–471, doi: 10.2514/3.25487.

[14] J. Heiligers, M. Ceriotti, C. R. McInnes, J. D. Biggs, Mission analysis and systems design of a near-term and far-term pole-sitter mission, Acta Astronautica 94 (1) (2014) 455–469, doi: 10.1016/j.actaastro.2012.12.015.

[15] P. Janhunen, A. A. Quarta, G. Mengali, Electric solar wind sail mass budget model, Geoscientific Instrumentation, Methods and Data Systems 2 (1) (2013) 85–95, doi: 10.5194/gi-2-85-2013.

[16] L. Mazal, P. Gurfil, Cluster flight algorithms for disaggregated satellites, Journal of Guidance, Control, and Dynamics 36 (1) (2013) 124–135, doi: 10.2514/1.57180.

[17] J. Mu, S. Gong, J. Li, Coupled control of reflectivity modulated solar sail for geosail formation flying, Journal of Guidance, Control, and Dynamics 38 (4) (2015) 740–751, doi: 10.2514/1.G000117.

[18] G. Aliasi, G. Mengali, A. A. Quarta, Special orbits for Mercury observation, in: V. Badescu, K. Zacny (Eds.), Inner Solar System - Prospective Energy and Material Resources, Springer International Publishing, 2015, Ch. 5, pp. 101–126, ISBN: 978-3-319-19568-1.

[19] F. Salazar, O. Winter, E. Macau, J. Masdemont, G. Gómez, Zero drift regions and control strategies to keep satellite in formation around triangular libration point in the restricted sun-earth-moon scenario, Advances in Space Research 56 (7) (2015) 1502–1518, doi: 10.1016/j.asr.2015.07.001.

[20] S. Gong, H. Baoyin, J. Li, Solar sail formation flying around displaced solar orbits, Journal of Guidance, Control, and Dynamics 30 (4) (2007) 1148–1152, doi: 10.2514/1.24315.

[21] S. Gong, H. Baoyin, J. Li, Relative orbit design and control of formation around displaced solar orbits, Aerospace Science and Technology 12 (2) (2008) 195–201, doi: 10.1016/j.ast.2007.05.004.

[22] W. Wang, J. Yuan, G. Mengali, A. A. Quarta, Invariant manifold and bounds of relative motion between heliocentric displaced orbits, Journal of Guidance, Control and Dynamics 39 (8) (2016) 1764–1776, doi: 10.2514/1.G001751.

[23] W. Wang, G. Mengali, A. A. Quarta, J. Yuan, Extreme values of relative distances for spacecraft in elliptic displaced orbits, Advances in Space Research 58 (4) (2016) 475–487, doi: 10.1016/j.asr.2016.05.007.

[24] W. Wang, G. Mengali, A. A. Quarta, J. Yuan, Analysis of relative motion in non-Keplerian orbits via modified equinoctial elements, Aerospace Science and Technology 58 (2016) 389–400, doi: 10.1016/j.ast.2016.09.001.

[25] K. Yamaguchi, H. Yamakawa, Study on orbital maneuvers of electric sail with on-off thrust control, Aerospace Technology Japan 12 (2013) 79–88, doi: 10.2322/astj.12.79.

[26] A. A. Quarta, G. Mengali, Minimum-time trajectories of electric sail with advanced thrust model, Aerospace Science and Technology 55 (2016) 419–430, doi: 10.1016/j.ast.2016.06.020.

[27] W. Wang, G. Mengali, A. A. Quarta, J. Yuan, Formation flying for electric sails in displaced orbits. Part II: Distributed coordinated control, Advances in Space Research .

[28] P. Toivanen, P. Janhunen, J. Envall, S. Merikallio, Electric solar wind sail control and navigation, Advances in the Astronautical Sciences 145 (2012) 275–285 .
[29] P. K. Toivanen, P. Janhunen, Spin plane control and thrust vectoring of electric solar wind sail, Journal of Propulsion and Power 29 (1) (2013) 178–185, doi: 10.2514/1.B34330.
[30] L. Niccolai, A. A. Quarta, G. Mengali, Electric sail elliptic displaced orbits with advanced thrust model, (in press). Acta Astronautica doi: 10.1016/j.actaastro.2016.10.036.
[31] L. Niccolai, A. A. Quarta, G. Mengali, Electric sail-based displaced orbits with a refined thrust model, (in press). Proceedings of the Institution of Mechanical Engineers, Part G: Journal of Aerospace Engineering doi: 10.1177/0954410016679195.
[32] K. Alfriend, S. R. Vadali, P. Gurfil, J. How, L. Breger, Spacecraft formation flying: Dynamics, control and navigation, Elsevier, Oxford, 2010, Ch. 2.
[33] H. Schaub, Relative orbit geometry through classical orbit element differences, Journal of Guidance, Control, and Dynamics 27 (5) (2004) 839–848, doi: 10.2514/1.12595.
[34] F. Jiang, J. Li, H. Baoyin, Y. Gao, Study on relative orbit geometry of spacecraft formations in elliptical reference orbits, Journal of Guidance, Control, and Dynamics 31 (1) (2008) 123–134, doi: 10.2514/1.30394.
[35] Z. Dang, Z. Wang, Y. Zhang, Modeling and analysis of the bounds of periodical satellite relative motion, Journal of Guidance, Control, and Dynamics 37 (6) (2014) 1984–1998, doi: 10.2514/1.G000259.

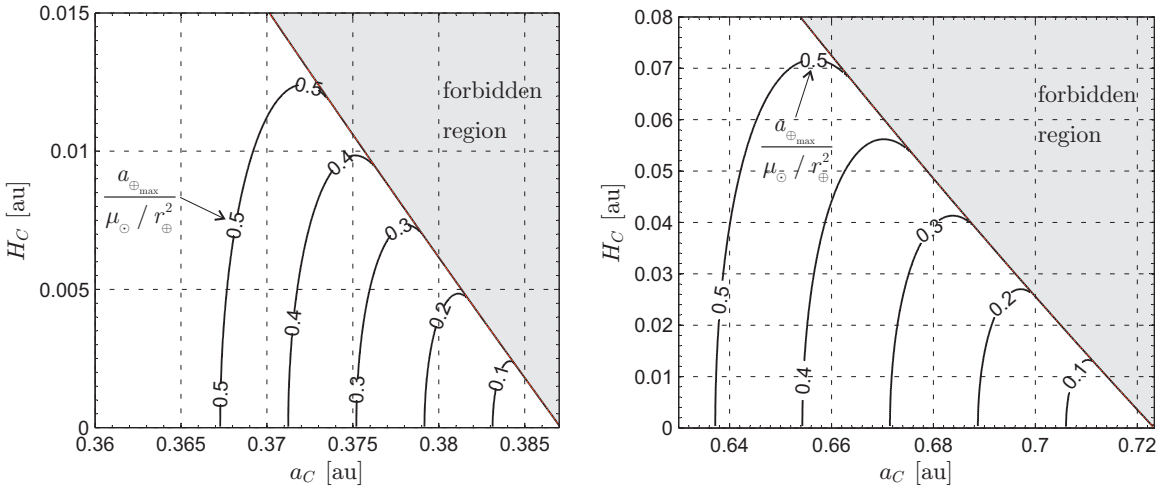

(a) Mercury.

(b) Venus.

(c) Earth.

(d) Mars.

(e) Jupiter.

(f) Saturn.

Figure 3: Feasible regions and contour lines of maximum value of characteristic accelerations $a_{\oplus\,\max}$ as a function of H_C and a_C for some reference celestial bodies.

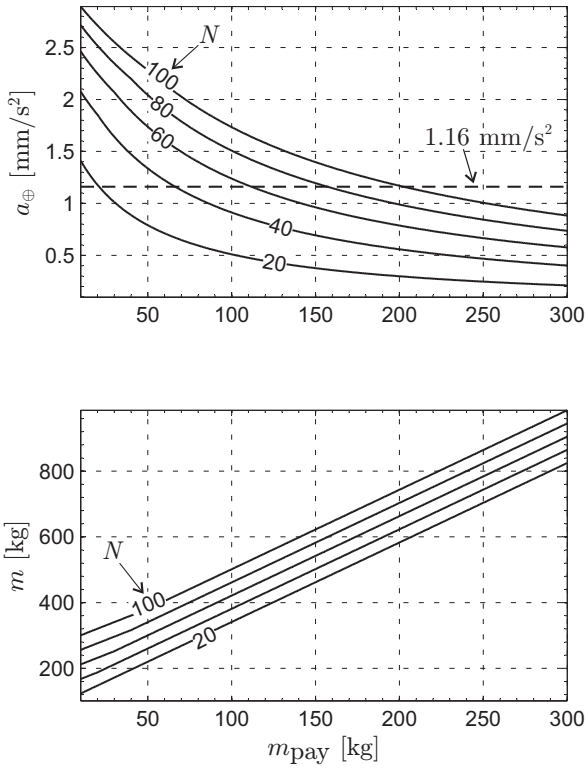

Figure 4: Characteristic acceleration $a_\oplus$ and total spacecraft mass m as a function of the payload mass m_{pay} and number of tethers N.

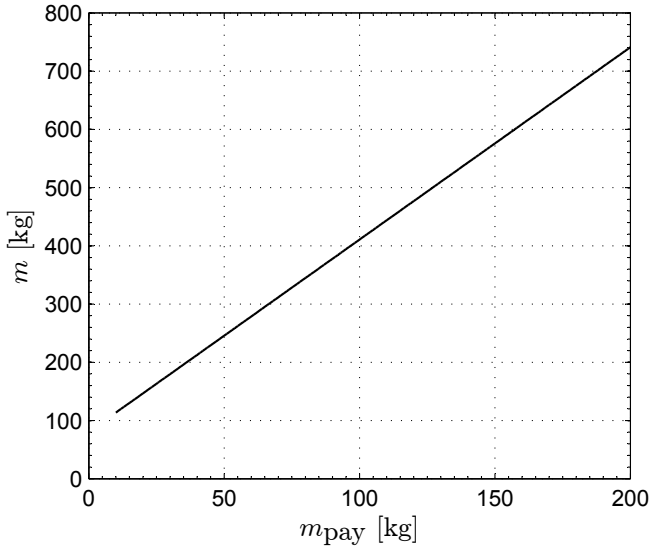

Figure 5: Total spacecraft mass m as a function of the payload mass m_{pay} when $a_\oplus = 1.16\,\mathrm{mm/s^2}$.

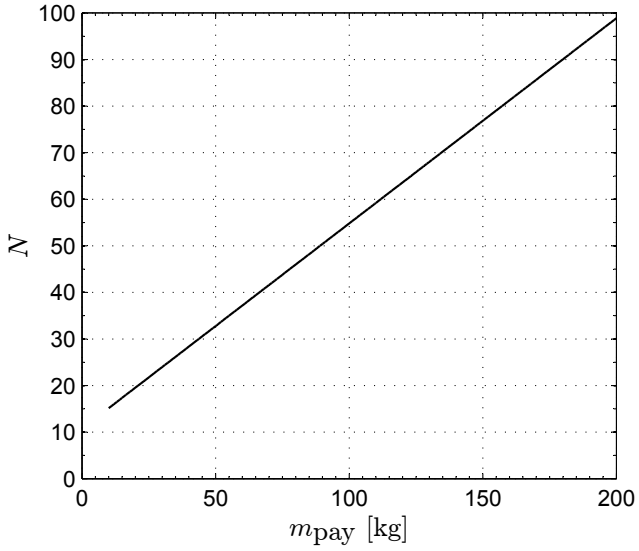

Figure 6: Number of tethers N as a function of the payload mass m_{pay} when $a_{\oplus} = 1.16\,\mathrm{mm/s^2}$.

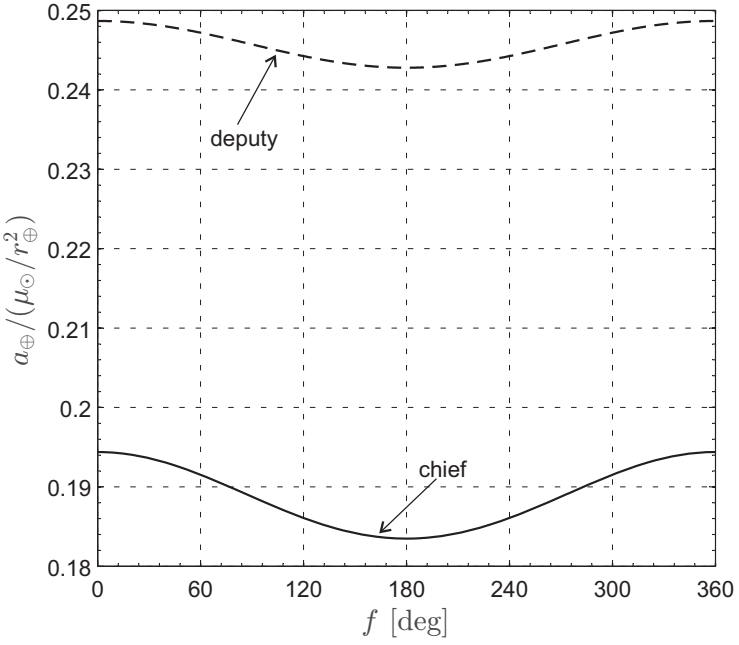

Figure 7: Characteristic accelerations of the chief and deputy as a function of the spacecraft true anomaly.

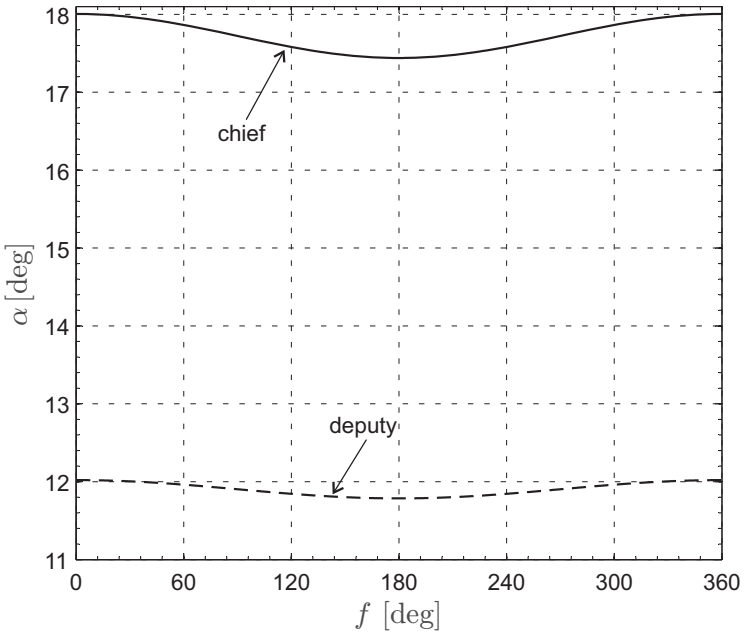

Figure 8: Pitch angles of the chief and deputy as a function of the spacecraft true anomaly.

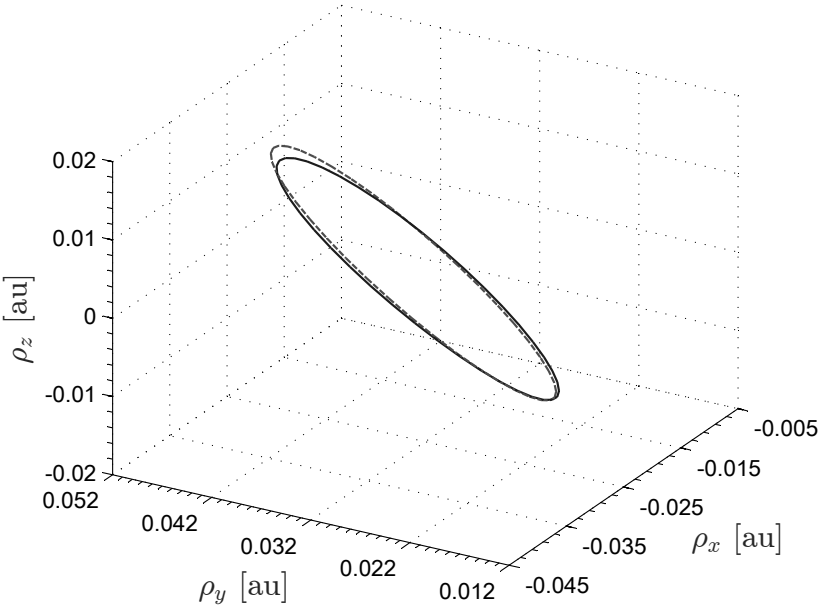

Figure 9: Spacecraft relative trajectory: approximate (dashed line) vs. reference solution (solid line).

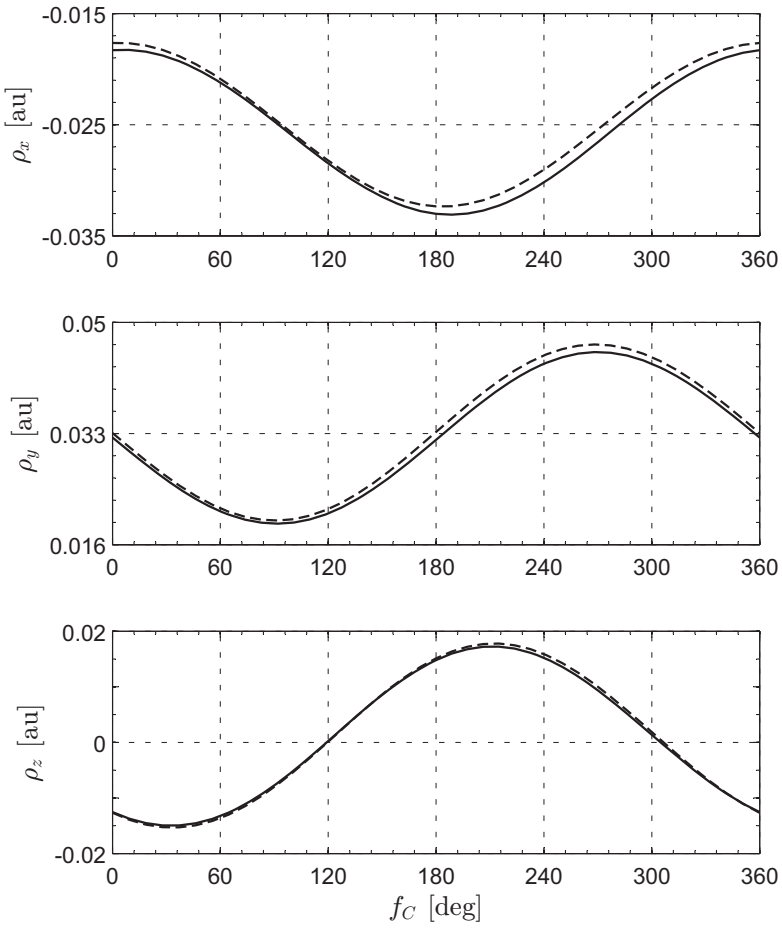

Figure 10: Comparison between the reference (solid line) and approximate (dashed line) solution as a function of the spacecraft true anomaly.

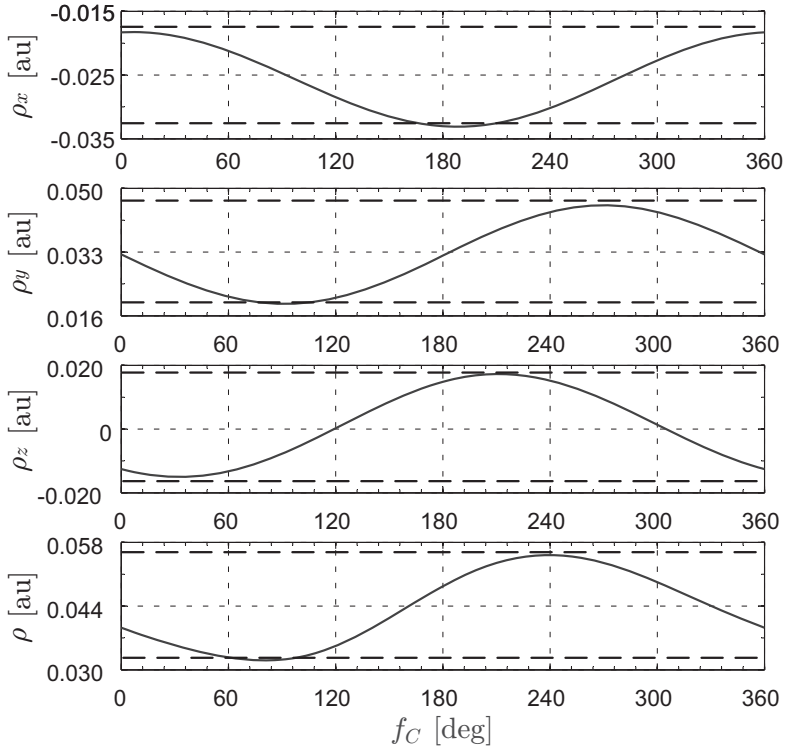

Figure 11: Approximate bounds (dashed lines) and simulated reference directional relative motion (solid lines).

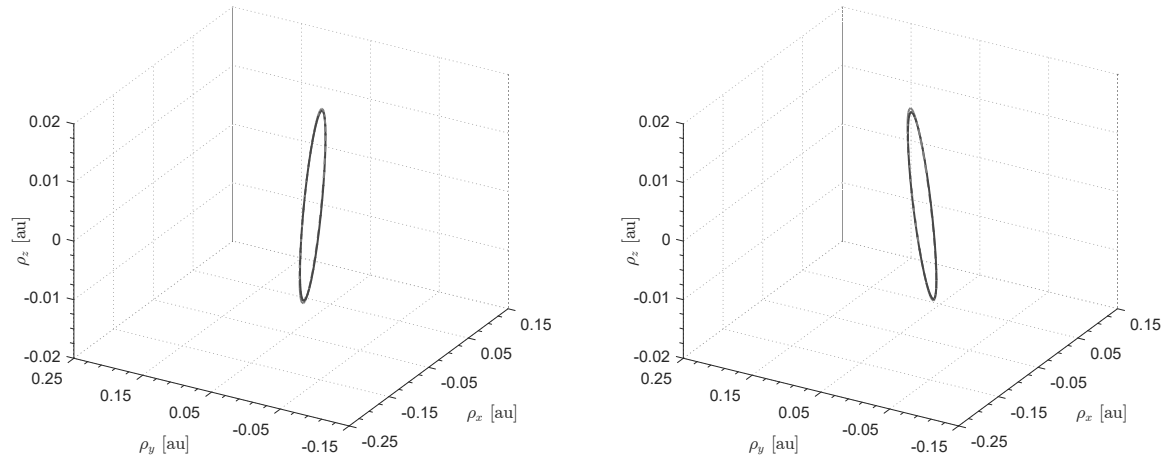

(a) $e_C = 0$ (b) $e_C = 0.02$

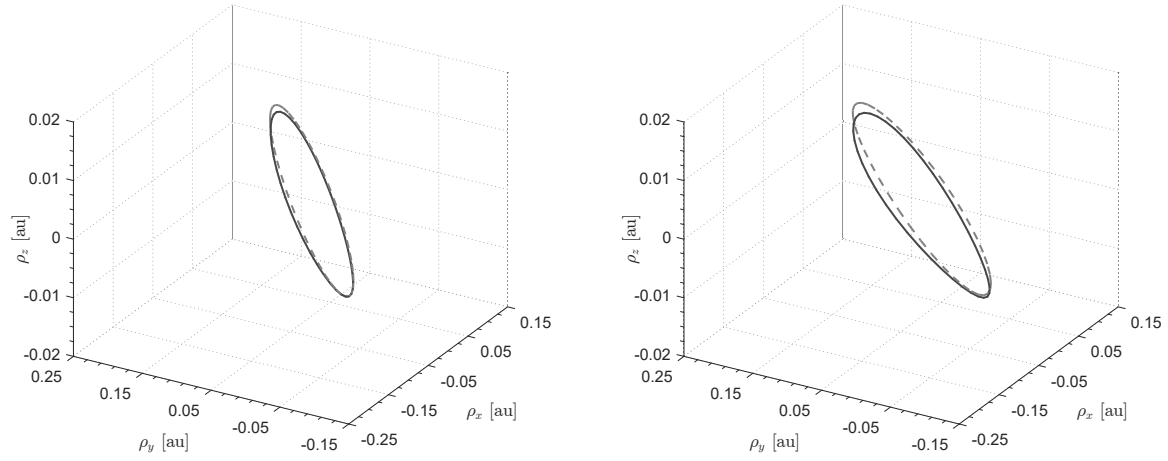

(c) $e_C = 0.04$ (d) $e_C = 0.06$

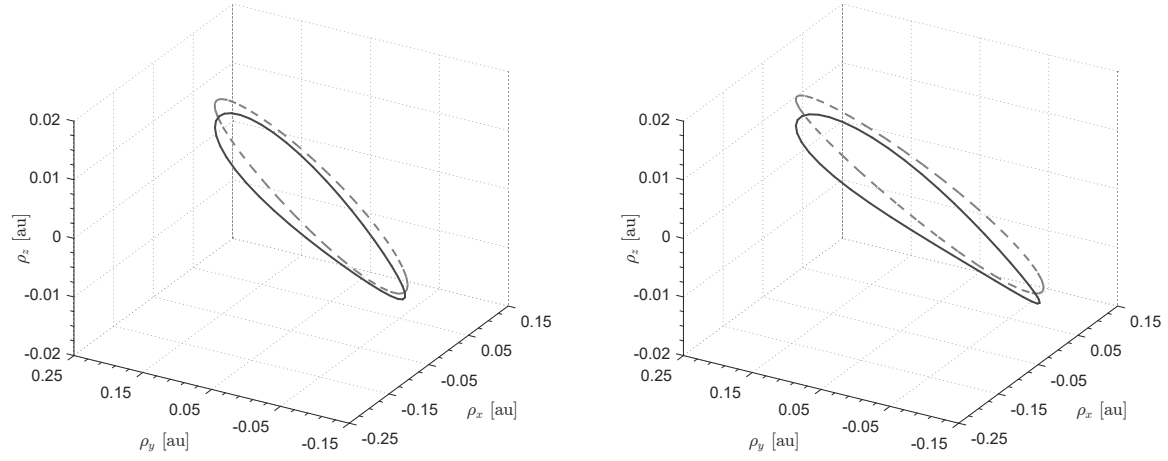

(e) $e_C = 0.08$ (f) $e_C = 0.1$

Figure 12: Spacecraft relative trajectory (solid line: reference; dashed line: approximate) as a function of the chief's eccentricity e_C.

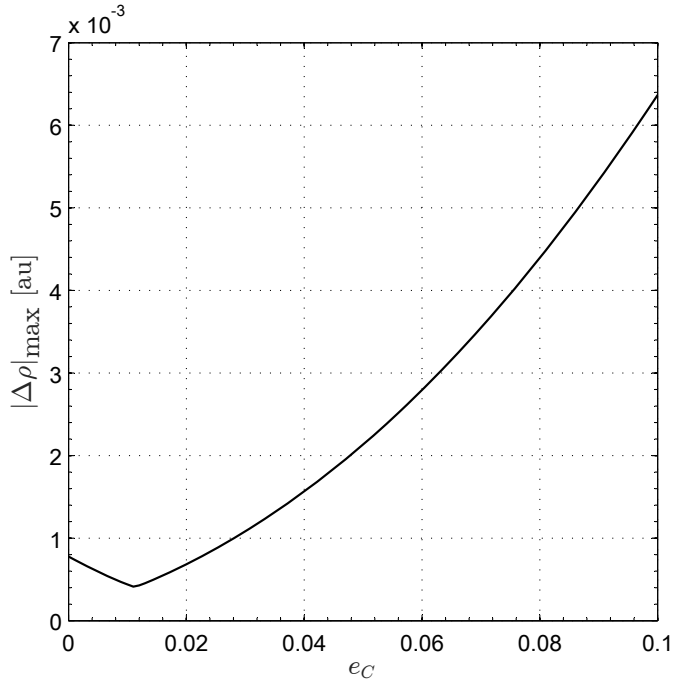

Figure 13: Maximum error (in modulus) achievable with the approximate solution as a function of the orbital eccentricity.